Control and Regulation of Mitochondrial Energetics in an Integrated Model of Cardiomyocyte Function

Sonia Cortassa,[†‡*] Brian O'Rourke,[†] Raimond L. Winslow,[‡] and Miguel A. Aon[†]
[†]Division of Cardiology, Johns Hopkins University, School of Medicine, and [‡]Institute for Computational Medicine, Baltimore, Maryland

ABSTRACT Understanding the regulation and control of complex networks of reactions requires analytical tools that take into account the interactions between individual network components controlling global network function. Here, we apply a generalized matrix method of control analysis to calculate flux and concentration control coefficients, as well as response coefficients, in an integrated model of excitation-contraction (EC) coupling and mitochondrial energetics (ECME model) in the cardiac ventricular myocyte. Control and regulation of oxygen consumption (V_{O2}) was first assessed in a mitochondrion model, and then in the integrated cardiac myocyte model under resting and working conditions. The results demonstrate that in the ECME model, control of respiration is distributed among cytoplasmic ATPases and mitochondrial processes. The magnitude of control by cytoplasmic ATPases increases under working conditions. The model prediction that the respiratory chain exerts strong positive control on V_{O2} (control coefficient 0.89) was corroborated experimentally in cardiac trabeculae utilizing the inhibitor titration method. In the model, mitochondrial respiration displayed the highest response coefficients with respect to the concentration of cytoplasmic ATP. This was due to the high elasticity of ANT flux toward ATP in the cytoplasm. The analysis reveals the complex interdependence of sarcolemmal, cytoplasmic, and mitochondrial processes that contribute to the control of energy supply and demand in the heart. Moreover, by visualizing the structure of control of the metabolic network of the myocyte, we provide support for the emerging concept of *control by diffuse loops*, in which action on the network (e.g., by a pharmacological agent) may bring about changes in processes without obvious direct mechanistic links between them.

INTRODUCTION

Since the chemiosmotic hypothesis was formulated, mechanism(s) involved in the control and regulation of energy supply and demand in the heart have been subject to intense scrutiny and debate. After many years of research, there is currently no consensus about the mechanism(s) and relative importance of the processes involved in matching energy supply with demand in the heart (for a review of the subject see (1,2)).

The complexity of the issue stems from the fact that mitochondrial energetics both modulates and is modulated by the network of mechano-electrical processes existing in the heart. In the past, most studies on this subject have considered only the major processes in isolation (e.g., mitochondrial energetics, electrophysiology, etc.). Consequently, it has been difficult to examine, in an intact system, whether the mechanisms controlling mitochondrial energetics differ depending on whether the muscle is at rest or is under working conditions. A computational model integrating both mitochondrial energetics and excitation-contraction (EC) coupling thus provides an important tool to address basic questions of energy supply and demand matching in the heart. Based on currently available evidence, it is likely that there is more than one mechanistic path implicated in metabolic control. On the one hand, mitochondrial Ca^{2+} appears to be a main regulator of energy production, presumably through the activation of Ca^{2+}-sensitive dehydrogenases. However, the Frank-Starling relation emphasizes that large changes in work and ATP production can occur in response to varying preload on the ventricle without substantial changes in the cytosolic Ca^{2+} transient, suggesting a mechanism involving ADP and classical respiratory control that is independent of Ca^{2+} (1). A combination of both regulatory mechanisms is needed to account for the ability of the heart to maintain NADH balance and ATP production under various conditions (1,2).

To quantitatively assess the mechanism(s) involved in matching energy supply with demand in the heart, mathematical models, applied together with direct experimentation, provide a way to understand the complex interactions of the many processes involved in EC-bioenergetic coupling. Over the past several years, we have developed and validated a computational model of the ventricular cardiomyocyte which integrates excitation-contraction coupling (EC coupling) and mitochondrial energetics, and which can simulate experimentally observed changes in force and oxygen consumption rates in cardiac muscle when challenged by an increase in workload (such as during an increase in stimulation frequency). This model, referred to as the excitation-contraction coupling and mitochondrial energetics (ECME) model, reproduces the steady-state and transient behavior of NADH and Ca^{2+} in the mitochondrial matrix, clarifying the parallel regulatory role of Ca^{2+} and ADP in matching energy supply and demand (3,4).

In this work, we apply the stoichiometric matrix method of Reder (5) to analyze the role of sarcolemmal, cytoplasmic, and mitochondrial process in the control of oxidative phosphorylation in the cardiomyocyte. This method generalizes earlier metabolic control analysis tools (6–8). Calculations of the control and response coefficient matrices and changes

Submitted August 6, 2008, and accepted for publication December 1, 2008.

*Correspondence: scortas1@jhmi.edu

Editor: Herbert Levine.

0006-3495/09/03/2466/13 $2.00

doi: 10.1016/j.bpj.2008.12.3893

in steady-state fluxes induced by perturbations of the system permit a deeper understanding of the relationship among the electrophysiological, Ca^{2+} handling, contractile, and metabolic components of the ECME model.

A glossary of terms used in this article is supplied as Table 1.

COMPUTATIONAL AND EXPERIMENTAL METHODS

Fig. 1 depicts a general scheme of the ECME model describing EC coupling (in guinea pig ventricular myocytes) (9,10) and mitochondrial energetics (3,11). In this model, EC coupling and energetics are linked through the concentrations of ATP, ADP, creatine, and creatine phosphate as well as mitochondrial and cytoplasmic Ca^{2+} and Na^{+}. The mitochondrial energetic model considers separately proton (V_{HNe}) and electron transport (V_{O2}) functions of the respiratory chain as well as the fluxes associated with phosphorylation (V_{ATPase}) and the proton pumping (V_{Hu}) across the mitochondrial F_1, F_0 ATP synthase (11,12). Despite being tightly coupled, the distinction between, e.g., V_{O2} and V_{HNe}, has the advantage of enabling the computation of molecular slip or intrinsic uncoupling that accounts for chemical reactions not coupled to proton translocation in oxidative phosphorylation (13,14).

The electrophysiological module includes the main ion transport processes involved in EC coupling. It accounts for Ca^{2+}, Na^{+}, and K^{+} currents across the sarcolemma, Ca^{2+} transport within the sarcoplasmic reticulum (SR) and across the SR membrane, and Ca^{2+} handling by mitochondria. Five different Ca^{2+} compartments are defined including the mitochondrial matrix, the dyadic subspace, the junctional and network SR, and the cytoplasmic space.

TABLE 1 Glossary

ADP_m	Mitochondrial ADP
ANT	Adenine nucleotide translocator
CK	Creatine kinase
C_o	Flux control coefficient in the absence of inhibitor
CrP	Creatine phosphate
$D_x v$	Elasticity matrix
EC	Excitation contraction
ECME	EC coupling-mitochondrial energetics
E_o	Total concentration of enzyme interacting with inhibitor
I_{Cab}	Background Ca^{2+} current
Id_r	Identity matrix of dimension r
I_{NaK}	Current through the Na^+ K^+ ATPase
I_{NCX}	Current through the sarcolemmal Na^+ Ca^{2+} exchanger
J_i	Flux in the presence of saturating levels of inhibitor
J_o	Flux in the absence of inhibitor
K_D	Inhibitor dissociation constant
L	Link matrix
N_r	Reduced stoichiometric matrix
SR	Sarcoplasmic reticulum
$V_{AM\text{-}ATP}$	Rate of myofibrillar ATPase
V_{ANT}	Rate of adenine nucleotide translocator
V_{ATPsy}	Rate of mitochondrial ATP synthase
V_{Cauni}	Rate of mitochondrial Ca^{2+} uniporter
V_{HFe}	Rate of succinate-driven proton pumping
V_{HNe}	Rate of respiratory chain proton pumping
V_{Hu}	Rate of proton pumping through ATP synthase
V_{leak}	Rate of proton leak
V_{NCE}	Rate of mitochondrial Na^+ Ca^{2+} exchanger
V_{O2}	Rate of oxygen consumption
V_{PMCA}	Rate of sarcolemmal Ca^{2+} ATPase
V_{RC}	Rate of respiratory electron transport
V_{TCA}	Rate of the tricarboxylic acid cycle
$\Delta\Psi_m$	Mitochondrial membrane potential

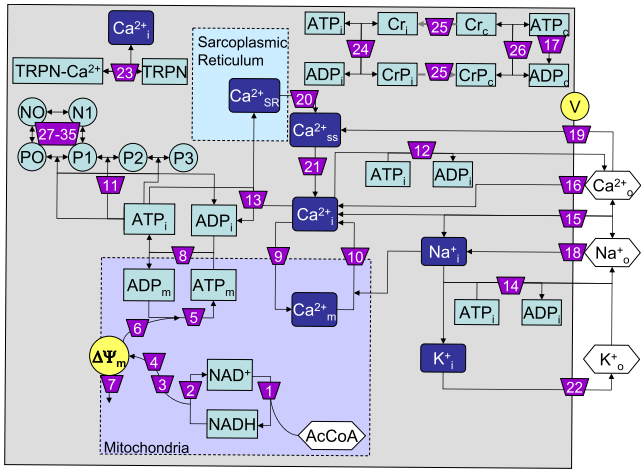

FIGURE 1 Scheme of the model ECME subjected to control analysis. The scheme shows mass transformation interactions between the state variables of the ECME model. For simplicity, regulatory interactions were omitted in the scheme (see Computational and Experimental Methods). State variables are indicated in rectangular (ion or metabolites) or circular (myofibril conformations) boxes. Boxes depict a light-blue background when the state variables participate in conservation relationships (ATP/ADP, Cr/CrP, NAD^+/NADH, TRPN/TRPN-Ca, and the various conformations of myofibrils). Ionic species are indicated on a dark-blue background. Hexagonal boxes denote inputs (ions or carbon substrate) that correspond to parameters in the model. Arrowheads point to the products of the numbered processes, whereas lines without arrowheads indicate inputs to those processes. In mitochondria, the TCA cycle was considered as a single step in the stoichiometric matrix; however, for the quantitation of the elasticity coefficients of the TCA cycle with respect to the intermediates, the disaggregated individual rate expressions, and their dependence with respect to $Ca^{2+}{}_m$, NAD^+, NADH, ADP_m, and ATP_m were taken into account. The individual elasticities were then added together to compute the overall elasticity of the TCA cycle with respect to each state variable, such that the stoichiometric matrix and that of elasticity coefficients are dimensionally consistent. The values V and $\Delta\Psi_m$ correspond to sarcolemmal and mitochondrial membrane potentials, respectively. See Table 2 for process key. The source code of the ECME model is available for download from http://senselab.med.yale.edu/ModelDB/ShowModel.asp?model=105383.

The mitochondrial module describes the production (F_1, F_O ATPase) and transport (15) of ATP, Ca^{2+} transport, and the activation of TCA cycle dehydrogenases by Ca^{2+}. The creatine kinase (CK) reaction occurs near the mitochondria, and the CrP diffuses to the cytoplasmic compartment where another pool of CK catalyzes the regeneration of ATP_{ic} to fuel constitutive cytoplasmic ATPases. The main ATP-consuming processes related to EC coupling are the myofibrillar ATPase (AM_ATP), SERCA, the Na^+-K^+ ATPase (I_{NaK}), and the Ca^{2+} ATPase (PMCA).

Control analysis of the ECME model: theoretical approach

Control analysis

Control analysis was performed by applying the method developed by Reder (5) as adapted to the mitochondrial (11) or the ECME model (3). In the framework of metabolic control analysis, Reder developed a generalized linear algebraic method that provides a way of analyzing the sensitivity of metabolic systems to perturbations triggered by either a change in the internal state of the system or by the environment. Here, we applied this method to a system in which metabolism, ion transport, and mechanical function are coupled. Because the ECME model was constructed in a modular way, the method

can be applied with a higher or lower degree of detail or refinement. In this way, and depending on the question to be examined, the extent of control exerted by a module can be applied by zooming in and out.

The departure point of the analysis is the stoichiometric matrix, obtained from the set of differential equations of the model. The stoichiometric matrix defines the structural relationships between the processes and the intermediates participating in the metabolic network under consideration. The information contained in the stoichiometric matrix is independent of both the enzyme kinetics and the parameters that rule the dynamic behavior of the metabolic system.

The second piece of information required to perform control analysis is the elasticity matrix, defined by the dependence of each process in the metabolic network on the intermediates (e.g., ions or metabolites) included in the model. The elasticity matrix is quantified through the derivatives of the rates of individual processes with respect to each possible effector. Each elasticity coefficient reflects the local property of a process; for example, an enzyme activity with respect to its substrate, which is linked to the global behavior of the system through the steady-state levels of metabolites (substrates or effectors) that intervene in the network dynamics.

By applying matrix algebra, the matrices corresponding to control and response coefficients are obtained. Both kinds of matrices quantify the relationships between control and regulation, respectively, in the network of reactions. The regulation exerted by internal or external effectors to a network can be quantified by the response coefficient (16).

The following matrix relationships were used in the computation of flux and metabolite concentration control coefficients,

$$C = Id_r - D_x v\, L \left(N_r\, D_x v\, L\right)^{-1} N_r, \quad (1)$$

$$\Gamma = -L \left(N_r\, D_x v\, L\right)^{-1} N_r, \quad (2)$$

with C and Γ referring to the flux- and metabolite concentration control coefficients, respectively; Id_r, the identity matrix of dimension r, the number of processes in the network under study; $D_x v$ the elasticity matrix; N_r the reduced stoichiometric matrix; and L, the link matrix that relates the reduced- to the full-stoichiometric matrix of the system. (For a more detailed description of Eqs. 1 and 2, see the Appendices.)

The advantages of the matrix method of Reder (5) over similar tools developed by others (7,8) is that: 1) it can be applied to networks of any complexity, including conserved cycles or multiple branches, and hierarchical relationships (17); and 2), it is not based on the compliance of the theorems of metabolic control analysis and the particular conditions under which the analysis is carried out.

Illustratively, the matrices used in the case of the isolated mitochondrial model for calculating the control and response coefficients are presented in the Appendices. The reactions of the TCA cycle, both in the mitochondrial or the ECME model, have been lumped into a single step. However, the regulatory interactions involved in each step of the TCA cycle were explicitly taken into account and the individual elasticities were added for consistency in the dimensions of the network matrices (see also legend of Fig. 1).

Control under resting and working conditions

We simulated the steady-state behavior of the ECME model under resting (i.e., no stimulation) and voltage-clamp (working) conditions. The voltage-clamp condition corresponds to successive 2 Hz cycles during which membrane potential is clamped at +10 mV for 200 ms followed by a voltage clamp at −80 mV for 300 ms. The average value of state variables and fluxes calculated during the last 100 ms at +10 mV were used to perform the control analysis. The (pseudo) steady-state value of the state variables so-determined were used to calculate the elasticity coefficients. In most cases, the elasticity coefficients could be determined analytically (when the rate expression is a direct function of the concentrations or levels of the variables, i.e., sarcolemmal or mitochondrial membrane potential) or numerically (when the rate expression of, e.g., a channel current, is a function of additional variables such as gating probabilities that are not amenable to algebraic computation). Once the elasticity and stoichiometric matrix were calculated, the system was algebraically manipulated with the linear algebra package of Maple 11 (Maplesoft, Waterloo, CA).

TABLE 2 Processes accounted for by the ECME model, numbered according to the keys in the table

Number	Abbreviation	Name
1	TCA	Tricarboxylic acid cycle
2	V_{RC}	Respiratory electron transport
3	HNe	Respiratory chain proton pumping
4	HFe	Succinate-driven proton pumping
5	ATPsy	Mitochondrial ATP synthase
6	Hu	Proton pumping through ATP synthase
7	Leak	Proton leak
8	ANT	Adenine nucleotide translocator
9	Ca_{uni}	Mitochondrial Ca^{2+} uniporter
10	V_{NCE}	Mitochondrial Na^+ Ca^{2+} exchanger
11	AM-ATP	Myofibrillar ATPase
12	PMCA	Sarcolemmal Ca^{2+} ATPase
13	SERCA	Sarcoplasmic reticulum Ca^{2+} ATPase
14	I_{NaK}	Current through the Na^+ K^+ ATPase
15	I_{NCX}	Current through the sarcolemmal Na^+ Ca^{2+} exchanger
16	I_{Cab}	Background Ca^{2+} current
17	$ATPase_c$	Constitutive cytosolic ATPase
18	I_{Na}	Na^+ inward currents
19	LCC	L type Ca^{2+} current
20	J_{Rel}	Ca^{2+} release from RyR
21	J_{xfer}	Ca^{2+} transport from subspace into cytoplasm
22	I_K	Outward potassium currents
23	—	Ca^{2+} association-dissociation to troponin
24	CK_i	Mitochondrial creatine kinase
25	—	Creatine species transport
26	CrKc	Cytosolic creatine kinase
27–35	—	Transitions between tropomyosin conformations

Experimental methods

Oxygen consumption determination in rat trabeculae

Rat cardiac trabeculae were excised and mounted in a force transducer, as described previously (3). The muscle was field-stimulated while being perfused with an oxygenated Krebs-Henseleit solution (in mM): 1.0 $CaCl_2$, 120 NaCl, 5.0 KCl, 2.0 $MgSO_4$, 1.2 $NaPO_4H$, 20 $NaHCO_3$, 10 glucose, pH 7.4. All experiments were carried out at 22°C. The rate of oxygen consumption was determined using an oxygen-sensitive fiber-optic sensor (Ocean Optics, Largo, FL). Oxygen consumption was measured with the sensor positioned within 100 μm of the muscle in the absence or presence of the indicated concentration of rotenone, a complex I inhibitor.

The control of mitochondrial respiration was assessed by titrating the respiratory flux with rotenone (concentrations ranging from 30 nM to 2.5 μM). After each increase in rotenone concentration, V_{O2} was measured as the slope of the O_2 decline upon brief cessation of flow of the perfusate. Since the muscle tissue was intact, we could not directly measure the extent of inhibition of complex I by rotenone. Thus, to quantify the control coefficient, we applied the method developed by Gellerich et al. (18), which is based on nonlinear regression analysis of inhibitor titration curves. The expression used to fit the inhibitor titration curve is

$$J = \frac{n \times \left(J_o - J_i\right)^2 \times E^n}{C_o \times J_o \times E_o^n + \left[\left(n - C_o\right) \times J_o - n \times J_i\right] \times E^n}, \quad (3)$$

where

$$E^2 + (K_D + I - E_o) \times E - K_D \times E_o = 0. \quad (4)$$

In Eq. 3, J is the measured flux at a given inhibitor concentration, J_o is maximal flux in the absence of inhibitor, and J_i is flow through the pathway with the enzyme completely inhibited; E is the concentration of free enzyme (variable according to the concentration of inhibitor, I,); E_o and K_D are the total concentration of enzyme and the dissociation equilibrium constant between enzyme and inhibitor, respectively; and C_o is the flux control coefficient in the absence of inhibitor. The empirical exponent n has been introduced in order not to be constrained by the rather restrictive linearity condition (18).

RESULTS

In this work, the term ''control'' indicates the extent to which a flux through a pathway, or the concentration of an intermediary metabolite, is altered by changing the activity of one or more steps, and will be quantified by flux and concentration control coefficients, respectively. The term ''regulation'' refers to how the flux of a pathway or a metabolite level is modified through the effect on the rate of an individual step by cellular factors, which may include intermediary metabolite concentrations, the ionic environment, etc., and will be quantified by the response coefficient. The response coefficient measures the fractional change in flux, e.g., respiration, in response to a fractional change in a parameter P (e.g., an effector such as Ca^{2+}) other than enzyme activity (16). The response of a pathway to an effector depends on two factors (19): 1), the extent of control exerted on the pathway by the enzyme that is the effector's target; and 2), the strength or elasticity of the effect of P on that enzyme. The response coefficient defined in this manner is the product of the control and elasticity coefficients. According to these definitions, metabolites or ions ''regulate'', whereas changes in enzyme activity or posttranslational modifications ''control''.

Control analysis of the mitochondrial energetics (ME) model

The control of mitochondrial energetics was first analyzed in the isolated mitochondrial model (11) in a similar parametric domain to that described below for the whole-cell integrated model to determine whether the control of energetics differed for isolated mitochondria and those interacting with the other subsystems of the cell.

The profile of control of V_{O2} by the different mitochondrial processes, the F_1,F_O ATP synthase, and the membrane potential ($\Delta\Psi_m$) are displayed in Fig. 2. V_{O2} is mainly controlled by the activity of the respiratory chain carriers (V_{RC}), the proton fluxes associated with respiratory electron transport (V_{HNe}), and ATP synthesis (V_{Hu}) (Fig. 2 *A*; see also (11): their Eqs. 26, 27, 31, and 32). By discriminating between V_{HNe} and V_{Hu}, we show that mitochondrial respiration is negatively controlled by the buildup of the proton motive force (V_{HNe}), and positively controlled by the flux of H^+ associated with ATP synthesis. As a caveat, the opposite pattern of control displayed by V_{RC} and V_{HNe} on V_{O2} should not be seen as being in conflict with respect to their acting as coupled processes; it only indicates that when the proton motive force is built up by V_{HNe}, it feeds back negatively on respiration. These effects also explain the positive and negative control displayed by V_{HNe} and V_{Hu}, respectively, on $\Delta\Psi_m$ (Fig. 2 *C*). Additionally, V_{O2} is significantly and positively controlled by the Ca^{2+} uniporter (V_{Cauni}) and the adenine nucleotide translocator (V_{ANT}) (Fig. 2 *A*). Minor

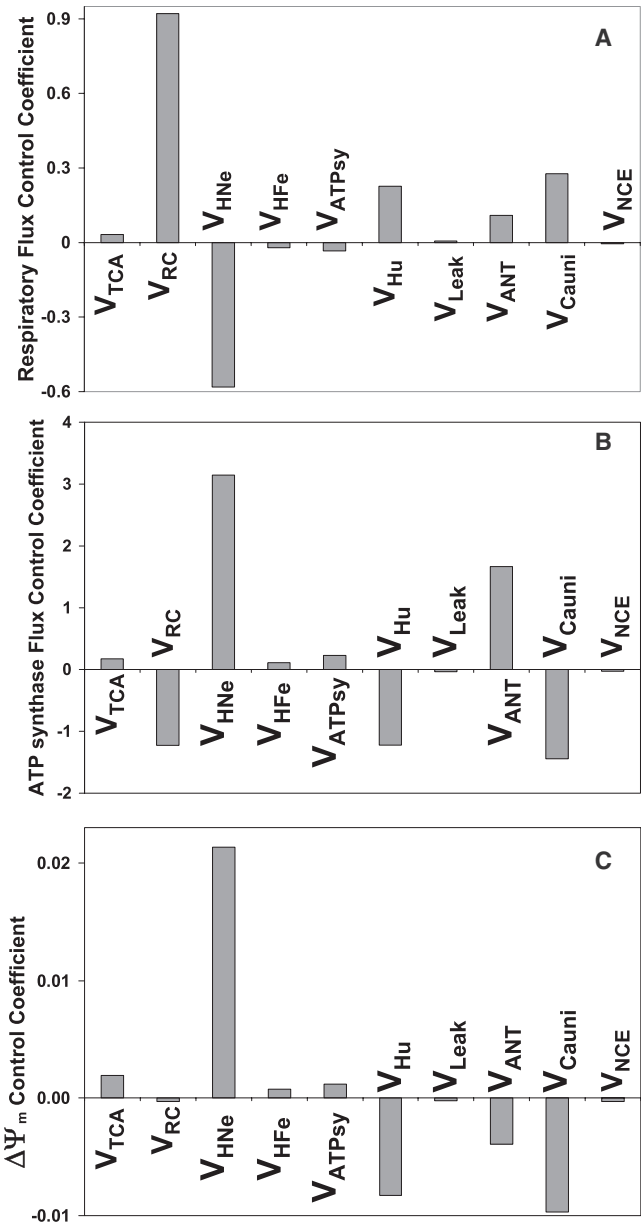

FIGURE 2 Metabolic fluxes and $\Delta\Psi_m$ control in the mitochondrial energetics model. V_{O2} stands for respiratory electron transport (from NADH to O_2) whereas V_{HNe} represents the respiratory proton translocation associated to V_{O2}. V_{HFe} represents the rate of proton translocation associated to succinate-driven respiration. (*A*) Control profile of the respiratory electron transport; (*B*) control of the ATP synthase; and (*C*) $\Delta\Psi_m$ control coefficients by each of the steps of the ME model (16).

positive control of respiration is contributed by the TCA cycle (V_{TCA}) and the proton leak (V_{leak}), and negative control of respiration is contributed by the proton flux associated with succinate-driven respiration (V_{HFe}) and the ATP synthase (V_{ATPsy}) (Fig. 2 *A*).

The ATP synthase control profile mirrors that of respiration, with the exception of V_{ANT} and the TCA cycle (V_{TCA}). For instance, V_{RC} and V_{HNe} exert negative and positive control, respectively, on V_{ATPsy} (Fig. 2, *A* and *B*). The positive control displayed by the ANT on V_{ATPsy} is due to the transport of ADP, the substrate for ATP synthesis, to mitochondria (Fig. 2 *B*), whereas in the case of respiration, the ANT exhibits positive control by dissipating $\Delta\Psi_m$, thereby accelerating respiration (Fig. 2 *A*). Accordingly, V_{ANT} displays negative control over $\Delta\Psi_m$ (Fig. 2 *C*). The profile of control of ATP synthesis mirrored that of the respiratory flux, due to $\Delta\Psi_m$ acting as the common intermediate. $\Delta\Psi_m$ exhibits a similar control profile as the ATP synthesis; both are controlled by the same processes and with the same sign but with different strengths (Fig. 2, *B* and *C*).

Ca^{2+} exerts two main effects in our model of mitochondrial energetics: 1), activation of the TCA cycle dehydrogenase activities that stimulate NADH production and respiration; and 2), dissipation of $\Delta\Psi_m$ by the transport processes, i.e., the Ca^{2+} uniporter (V_{Cauni}) and the Na^+ Ca^{2+} exchanger (V_{NCE}). In the case of V_{Cauni}-mediated Ca^{2+} transport, both the TCA cycle stimulation and the $\Delta\Psi_m$ dissipation contribute positively to control respiration, whereas V_{NCE} negatively controls respiration even though it dissipates $\Delta\Psi_m$ (Fig. 2, *A* and *B*) because the impairment of the stimulatory effect of Ca^{2+} on the TCA cycle dehydrogenases overrides the $\Delta\Psi_m$ dissipation by V_{NCE}.

The results presented in this section show that the control of energetics in isolated mitochondria and, more specifically, of the respiratory and ATP synthesis fluxes, is distributed. Control is shared by processes associated with adenine nucleotide production and transport, as well as by Ca^{2+} dynamics.

Control analysis of mitochondrial energetics integrated with EC coupling

In this section, we examine how the control profile of energetics is modified when mitochondria are integrated with EC coupling. To perform these studies, we quantified the structure of control and regulation of the network of reactions described by the ECME model (Fig. 1).

The calculations are performed under resting and working conditions. The latter condition is assessed by clamping the voltage at +10 mV until a pseudo-steady state is attained (see Control under Resting and Working Conditions, above). A voltage of +10 mV was chosen because it corresponds approximately to the plateau of the action potential. Contractile force is close to its maximum during the plateau phase, and the energy-consuming pumps are nearly at maximal work during the contraction cycle. Although this corresponds to a transient state of the myocyte beating cycle, it was chosen to represent the working state in our calculations.

Control of respiration

Control by mitochondrial processes. Fig. 3 *A* shows the distribution of flux control coefficients of V_{O2} by mitochondrial and cytoplasmic processes under similar parametric conditions as described above. Qualitatively, isolated and integrated mitochondria share the same rate-controlling steps (compare Fig. 2 *A* and Fig. 3 *A*). Quantitatively, the control in integrated mitochondria under resting conditions resembles that of the isolated mitochondria in state 4 (low ADP), in keeping with the low energy demand of the system.

As expected, the interaction between cytoplasmic and mitochondrial processes is quantitatively more important under working conditions. This is revealed by the control over respiration exerted by cytoplasmic ATP hydrolases, such as the

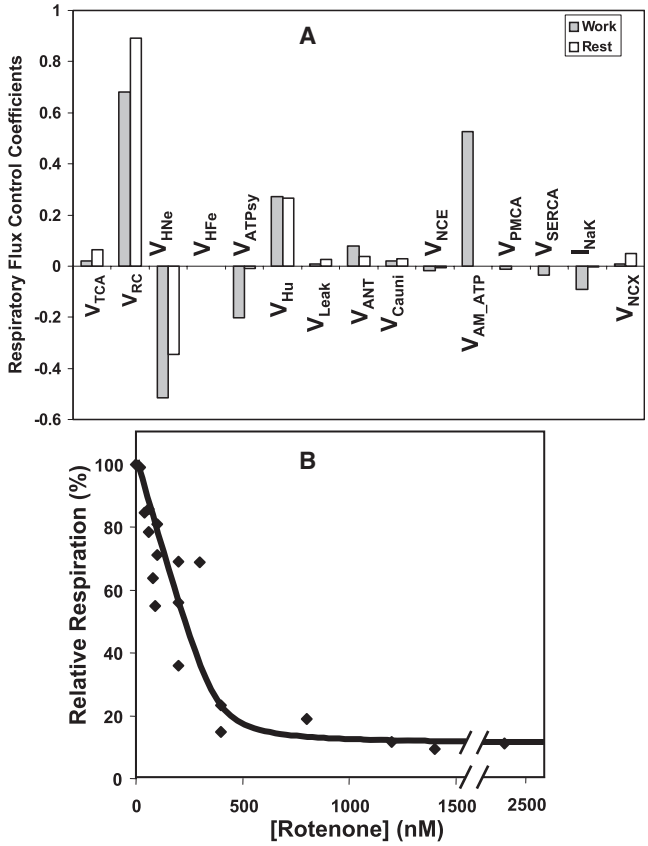

FIGURE 3 Control analysis of mitochondrial respiration in the ECME model and in rat trabeculae. (*A*) Control coefficients of mitochondrial and cytoplasmic processes on V_{O2} under resting or working conditions. The control of the electron transfer from NADH is calculated following the matrix method as indicated in Computational and Experimental Methods. (*B*) Rat trabeculae O_2 consumption flux titrated with the complex I inhibitor, rotenone. The data shown correspond to averages of three independent determinations performed in triplicate for each rotenone concentration. From these data a control coefficient of 0.89 was calculated based on the inhibitor titration method (18) (see Computational and Experimental Methods).

myofibrillar ATPase (V_{AM_ATP}), whose contribution to control is only significant during working conditions (Fig. 3 *A*).

Control of respiration is widely distributed among mitochondrial processes with V_{RC}, V_{HNe}, V_{ATPsy}, V_{Hu}, and V_{ANT} being quantitatively the most conspicuous, under both resting and working conditions. This is due to the control exerted by those processes on $\Delta\Psi_m$, which is a main effector of the respiratory flux (Fig. 3 *A*). The mitochondrial leak, V_{leak}, exhibits a larger control under resting than working conditions because its relative importance as a $\Delta\Psi_m$ consumer decreases during work. In the resting cell, the major rate-controlling processes of respiration were: $V_{RC} > V_{HNe} > V_{Hu} > V_{TCA} > V_{ANT} > V_{Cauni} > V_{leak}$, with a negative control exerted by the V_{NCE}, and insignificant control by V_{ATPsy}. During work, the most relevant rate-controlling steps were: $V_{RC} > V_{HNe} > V_{Hu} > V_{ATPsy} > V_{ANT} > V_{TCA} > V_{Cauni} > V_{NCE} > V_{leak}$ (Fig. 3 *A*).

Control by EC coupling processes. As noted earlier, the control of mitochondrial respiration by cytoplasmic processes is apparent only during work. The only EC coupling process that exerts some control over respiration under resting conditions is the sarcolemmal Na^+/Ca^{2+} exchanger (I_{NCX}), which influences Na^+ and Ca^{2+} levels in the cytoplasm, $\Delta\Psi_m$, and Na^+ and Ca^{2+} transport across the mitochondrial membrane.

Under working conditions, the respiratory flux is also controlled by the major cytoplasmic ATPases: $V_{AM\text{-}ATP}$, V_{SERCA}, I_{NaK}, and plasmalemmal Ca^{2+} ATPase (V_{PMCA}) (Fig. 3 *A*). While $V_{AM\text{-}ATPase}$ exerts a positive control on respiration, the others exhibit a negative control: $I_{NaK} > V_{SERCA} > V_{PMCA}$, because of their important effects on Ca^{2+} dynamics.

Experimental assessment of the control of mitochondrial respiration in intact tissue. This section is intended to illustrate how a particular control coefficient in the network may be subjected to experimental test to compare it with the calculated value. According to the control analysis calculations, the activity of the respiratory chain carriers (V_{RC}) exerts a strong control on V_{O2}. To verify this experimentally, rat heart trabeculae were subjected to 0.5 Hz field stimulation, and rotenone, an inhibitor of complex I of the respiratory chain, was titrated (Fig. 3 *B*). This inhibitor titration experiment rendered a control coefficient of 0.89 for the control of V_{O2} by the respiratory chain. This result is in quantitative agreement with the high control exhibited by the respiratory carriers in the control analysis of the ECME model (Fig. 3 *A*).

Control of ATP synthesis

Control by mitochondrial processes. When energy demand is low, flux of ATP synthesis can display larger variations than under working conditions when the ATP production is tightly committed to fulfilling the energy demand. This explains why values of the control coefficients for ATP synthesis are larger under resting than working conditions (Fig. 4). Mitochondrial ATP synthesis is positively controlled by the TCA cycle and the ANT, and negatively controlled by the respiratory chain activity (V_{RC}) and proton transport through the ATP synthase (V_{Hu}) (Fig. 4). As $\Delta\Psi_m$ consumers, the proton leak and NCE display negative control on ATP synthesis, whereas the Ca^{2+}uniporter exhibits a small amount of positive control at rest, but a negligible (slightly negative) effect under working conditions. ATP synthase is the only mitochondrial process that displays a higher degree of control on ATP production under working, rather than resting, conditions (Fig. 4).

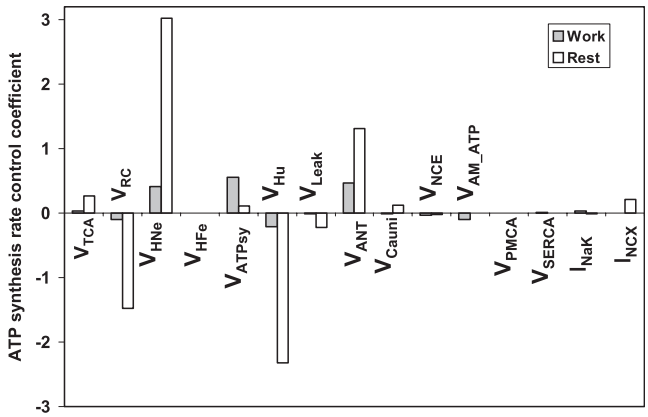

FIGURE 4 Control of the synthesis of ATP in the ECME model. The control coefficients of the rate of ADP phosphorylation, V_{ATPsy}, by each of the mitochondrial and several cytoplasmatic processes are displayed. The control coefficients were calculated by applying the matrix method described in Computational and Experimental Methods and in the Appendices.

Control by EC coupling processes. The AM-ATPase negatively controls the flux of ATP synthesis (Fig. 4). This seemingly counterintuitive result can be explained as control by diffuse loops mediated, in this case, by the decrease in ATP_i that an increase in AM-ATPase would bring about, in turn causing a decrease in the activity of the SERCA pump (see Discussion and Table 3, third row). Thus, AM-ATPase has a positive control on the concentration of $Ca^{2+}{}_i$ in the cytoplasm. The increase in $Ca^{2+}{}_i$ concentration resulting from the decrease in SERCA activity will, in turn, produce an increase of V_{Cauni}, transporting more Ca^{2+} into the mitochondria (also reflected by the large positive control of AM-ATPase on V_{Cauni}, not shown). The effect of the Ca^{2+} uniporter to dissipate $\Delta\Psi_m$ overrides the small positive

TABLE 3 Control of energetic variables through diffuse loops

Variable controlled	Controlling process	Intermediate variable	Intermediate process
Respiration	V_{AM_ATP}	$Ca^{2+}{}_m$	V_{SERCA}, V_{TCA}
	V_{Cauni} and V_{NCE}	$Ca^{2+}{}_m$	V_{TCA}
ATP synthesis (work condition)	V_{AM_ATP}	$Ca^{2+}{}_m$ and $\Delta\Psi_m$	V_{SERCA} and V_{Cauni}
	I_{NaK}	Na^+ and $Ca^{2+}{}_i$	I_{NCX}, V_{SERCA}, and V_{Cauni}
$Ca^{2+}{}_m$	V_{TCA}, V_{HNe}	$\Delta\Psi_m$	V_{NCE}, V_{Cauni}
ATP_i (work condition)	V_{SERCA}, I_{NaK}	$Ca^{2+}{}_i$	V_{AM_ATP}

control of the ANT brought about by the increase in ADP produced by the AM-ATPase. The net effect is a decrease of flux through the ATP synthase (Fig. 4).

As mentioned above for the AM-ATPase, the cytoplasmic ATPases exert their control on mitochondrial respiration and ATP synthesis by translating the direct effect on ATP_i into changes in $Ca^{2+}{}_i$ and $Ca^{2+}{}_m$ levels, which primarily impacts $\Delta\Psi_m$. Another example is the negative effect of an increase in Na^+ K^+ ATPase on respiration. The increase in Na^+ pump activity lowers intracellular Na^+, leading to an increased cellular extrusion of $Ca^{2+}{}_i$ via the sarcolemmal Na^+/Ca^{2+} exchanger (NCX). This decrease in $Ca^{2+}{}_i$ lessens the extent of $\Delta\Psi_m$ dissipation associated with mitochondrial Ca^{2+} transport, which results in a higher $\Delta\Psi_m$ and a decrease of respiration. The decrease in the flow through the electron transport chain is due to the inverse relationship between V_{O2} and $\Delta\Psi_m$, i.e., the higher the $\Delta\Psi_m$, the lower the respiratory flux. This is the main mechanism that drives mitochondria between states 3 (high respiration, low $\Delta\Psi_m$, high ADP) and 4 (low respiration, high $\Delta\Psi_m$, high ATP) under physiological conditions.

Regulation of mitochondrial respiration by the effectors Ca^{2+}, ATP, and ADP

The ECME model recapitulates the linearity between cardiac work and respiration in the heart (3) and the rapid time-dependent changes in mitochondrial NADH and $Ca^{2+}{}_m$ in response to abrupt changes in workload (3,11). The model incorporates Ca^{2+} and ADP as two important messengers that signal changes in cardiac work and modulate mitochondrial energy production. The dynamics is dependent on the balance between ADP-dependent stimulation of mitochondrial oxidative phosphorylation and Ca^{2+}-dependent activation of TCA cycle dehydrogenases. However, from a quantitative standpoint, it is unknown to what extent mitochondrial respiration is regulated by mitochondrial Ca^{2+} and ADP. To address this question, we calculated the response coefficients of energy fluxes to variations in Ca^{2+}, ATP, and ADP.

As can be seen in Table 4, ATP_i is the major regulatory intermediate. Mitochondrial ADP (ADP_m; not shown), and $Ca^{2+}{}_i$ contribute response coefficients that are smaller by several orders of magnitude. Interestingly, after ATP_i, the regulation conferred by $\Delta\Psi_m$ on key mitochondrial processes is the second most important factor, in terms of partial response coefficients (the partial response coefficient is defined in Appendix 1 by Eq. 8). However, in the computation of the total response coefficients (shown in Table 4), the terms corresponding to the respiratory chain and the ATP synthase cancel each other out, rendering very small total response coefficient values (see also Appendix 1).

TABLE 4 Response coefficients of respiration and ATP synthase with respect to regulatory intermediates

Condition	Work			Rest		
Intermediate	ATP_i	$Ca^{2+}{}_i$	$\Delta\Psi_m$	ATP_i	$Ca^{2+}{}_i$	$\Delta\Psi_m$
V_{O2}	-0.04	-2.10^{-11}	-1.10^{-9}	-0.01	4.10^{-10}	-2.10^{-8}
V_{HNe}	-0.05	0	-3.10^{-9}	-0.03	3.10^{-12}	-3.10^{-8}
V_{ATPsy}	-0.19	-8.10^{-12}	2.10^{-9}	-1	3.10^{-11}	3.10^{-7}
V_{Hu}	-0.17	-5.10^{-12}	5.10^{-9}	-0.02	5.10^{-12}	-9.10^{-9}

The response coefficient of flux J_i with respect to the intermediate x was calculated according to the expression $R_x^{J_i} = \sum_{\text{all } k} C_k^{J_i}\,\varepsilon_x^k$, being $C_k^{J_i}$ the flux control coefficient with respect to the activity of process k, and ε_x^k the elasticity of the rate of k with respect to the intermediate x, as defined in Ainscow and Brand (16) (see also Appendices).

Control of ATP_i, $Ca^{2+}{}_m$, and $\Delta\Psi_m$

Control by mitochondrial processes. Due to the relevance of ATP_i, $\Delta\Psi_m$, and $Ca^{2+}{}_m$ as main regulators of the respiratory flux, we looked closely at the processes controlling their levels.

Under working conditions, the control of ATP_i concentration is highly distributed with positive control exerted by $V_{ATPsy} > V_{ANT} > V_{HNe} > V_{Cauni} > V_{RC} > V_{TCA}$, and negative control by $V_{HU} > V_{NCE}$ (Fig. 5 *A*). As expected, the control of ATP_i by the ATP synthase was much higher under working than resting conditions, likely due to the large ATP demand associated with the contractile activity. However, at rest, the magnitude of control coefficients of most mitochondrial processes are larger than under working conditions, $V_{Cauni} > 2V_{HNe} > V_{Hu} > V_{TCA} > V_{leak}$, except for those of V_{RC} and V_{ANT}, which are similar under both conditions (Fig. 5 *A*). In most cases, the control of ATP_i by mitochondrial processes is mediated by $\Delta\Psi_m$ or $Ca^{2+}{}_m$. The V_{ANT} represents an exception to this pattern, despite being a $\Delta\Psi_m$ consumer, because it provides the substrate for ATP synthesis and transports the newly synthesized ATP to the cytoplasm.

Overall, with the notable exception of the control of $Ca^{2+}{}_m$ by the NCE and the ATP synthase, the magnitude of the control coefficients is larger under resting than under working conditions (Fig. 5 *B*). At rest, $Ca^{2+}{}_m$ is controlled largely by mitochondrial processes; only NCX and the background Ca^{2+} current serve to influence $Ca^{2+}{}_m$ in the absence of pacing (Fig. 5 *B*). $Ca^{2+}{}_m$ is negatively controlled by the TCA cycle, respiration, V_{NCE}, and the ANT, and positively by the leak, V_{Hu}, and the Ca^{2+} uniporter (Fig. 5 *B*). It may appear counterintuitive that processes that consume $\Delta\Psi_m$ result in an increase in Ca^{2+} accumulation in the mitochondrial matrix. This can be explained through the sensitivity (quantified by the elasticity coefficient) of the Ca^{2+} uniporter and NCE to $\Delta\Psi_m$; although both processes are dependent on $\Delta\Psi_m$, the stimulation of NCE activity will be larger than V_{Cauni} for a similar increase in $\Delta\Psi_m$. Thus, every process that contributes positively to building $\Delta\Psi_m$ exerts negative control over $Ca^{2+}{}_m$, as a consequence of the stimulation of Ca^{2+} efflux from mitochondria. On the contrary, processes that consume $\Delta\Psi_m$ positively control $Ca^{2+}{}_m$ (Fig. 5). As a consequence, the positive/negative control of mitochondrial processes on $Ca^{2+}{}_m$ depends upon an increase/decrease of the net mitochondrial uptake of Ca^{2+} due to consumption/buildup of $\Delta\Psi_m$, respectively.

The control of $\Delta\Psi_m$ by mitochondrial processes followed the expected pattern according to their ability to dissipate or

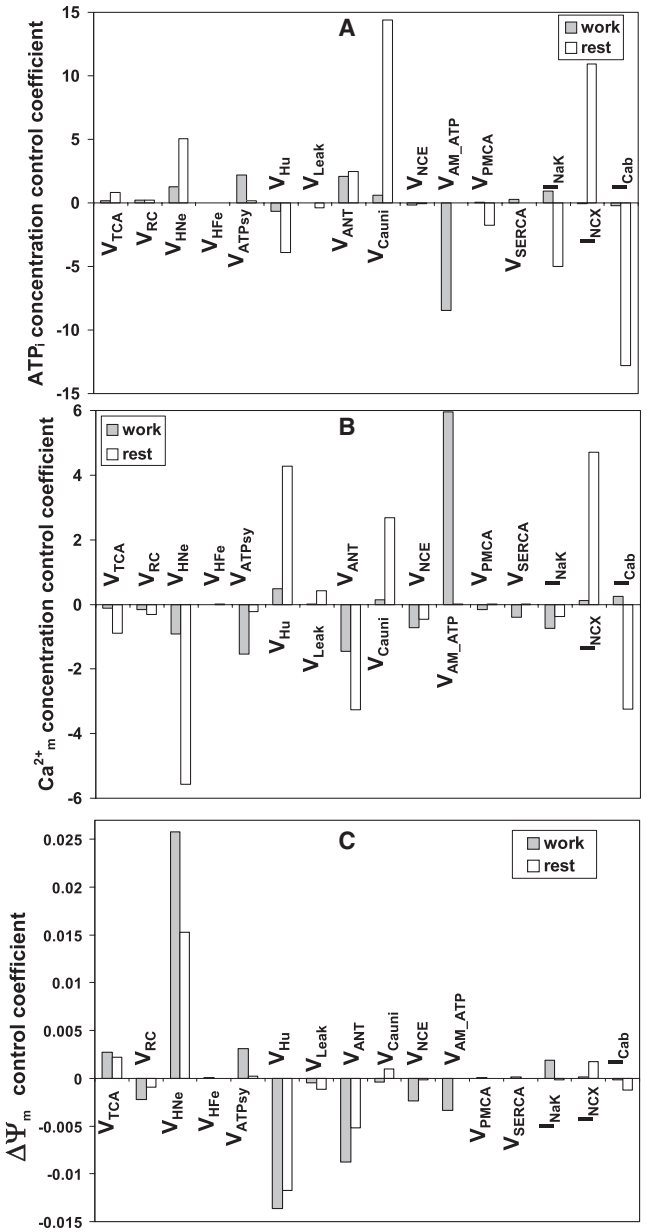

FIGURE 5 Control of ATP_i, $Ca^{2+}{}_i$ concentrations, and $\Delta\Psi_m$ in the ECME model. From the computation, under resting or working conditions of the matrix Γ of metabolite concentration control coefficients, the control coefficients of ATP_i (*A*), $Ca^{2+}{}_m$ (*B*), and $\Delta\Psi_m$ (*C*), are extracted.

build-up $\Delta\Psi_m$. Notably the magnitude of the control displayed by every process controlling $\Delta\Psi_m$ was much larger under working than resting conditions. This result speaks to the important role of $\Delta\Psi_m$ as a mediator of mitochondrial energy production.

Control by cytoplasmic processes. In the resting cardiomyocyte, only NCX and the background sarcolemmal Ca^{2+} current, I_{Cab}, exerted some positive and negative control, respectively, on the level of $Ca^{2+}{}_m$. This control may be explained through the same control pattern for ATP_i, which fuels the activity of PMCA, resulting in a decrease of $Ca^{2+}{}_m$. ATP_i is mainly consumed by the Na^+K^+ ATPase and PMCA under rest. This is a rather complex diffuse loop encompassing the ion transporters NCX, I_{Cab}, I_{NaK}, and PMCA, $Ca^{2+}{}_i$, and ATP_i as mediators of the effects on mitochondrial Ca^{2+}.

The main ATP consumer during work is the myofibrillar ATPase; thus, the negative control exerted by AM-ATPase on the ATP_i concentration can be readily understood. The other ATP-consuming processes such as the Na^+K^+ ATPase, SERCA, and PMCA display a positive control on ATP_i. This control is mediated by the negative control these ATPases exert on $Ca^{2+}{}_i$ that brings about ATP consumption by the myofibrils. The activities leading to a decrease in $Ca^{2+}{}_i$ result in an increase of ATP_i, irrespective of their ATP-consuming properties (Fig. 5). The opposite rationale applies to the effect of the NCX that, when studied at +10 mV, is operating in reverse mode, thus contributing to the increase of $Ca^{2+}{}_i$ as well as I_{Cab}.

DISCUSSION

The main goal of this work was to investigate in an integrated and quantitative manner the mechanisms of control and regulation of energy supply and demand in cardiomyocytes under resting and working conditions. This is the first time that such an attempt has been performed on a coupled network of enzyme reactions and ion transport processes to elucidate the interplay among energetic, electrical, Ca^{2+} handling, and contractile processes.

The following findings further illustrate the power and the potential of the approach undertaken: 1), the control of mitochondrial respiration was distributed across several mitochondrial processes in both the isolated and integrated models, with differences in the magnitude of the control coefficients; 2), when linked with EC coupling, mitochondrial respiration was additionally controlled by cytoplasmic ATPases; 3), the control profile was quantitatively different during resting and working conditions; 4), the highest response of mitochondrial respiration was to ATP_i, as a consequence of the high elasticity of the ANT toward ATP_i; and 5), control in this complex network was exerted through diffuse loops, often leading to counterintuitive conclusions.

The following three main features have emerged from previous analyses of control in metabolic networks (6,20,21); 1), control is distributed, as opposed to being concentrated in rate-limiting steps; 2), control changes both qualitatively (which site or step) and quantitatively (control strength) with the physiological conditions; and 3), there is a difference between control and regulation. All three findings are corroborated by this work, and further extended to show that in complex networks, control operates through diffuse loops.

Control of energy supply and demand in the ECME model

The analyses of Figs. 3 *A* and 4 are particularly instructive in answering the main question posed by the study. It can be seen

clearly that the control of energy supply and demand is highly distributed among mitochondrial and EC coupling processes. As expected, when the demand is higher (work condition) the control of the rate of mitochondrial respiration by cytoplasmic ATPases is also higher, especially the positive control exerted by the myofibrillar ATPase (Fig. 3 *A*). Moreover, we were able to show experimentally in working muscle that respiration through complex I is one of the main rate-controlling steps of the respiratory chain (Fig. 3 *B*). However, the model analysis (Figs. 3 *A* and 4) also revealed that the control of respiration and ATP supply depend on other processes, including some which exert negative control, e.g., the effects of the F_1,F_0 ATPase, V_{HNe}, and several cytoplasmic ATPases on respiration (Fig. 3 *A*). Thus, when analyzed as a whole, one cannot rely on one process in the network, not matter how quantitatively important it is.

The control of ATP synthesis is shared by most of the mitochondrial processes analyzed (Fig. 4). A reduction in the magnitude of most of these control coefficients under working conditions suggests that the range of variation of ATP production is more restricted when the energetic demand is large.

Regulation of energy supply and demand in the ECME model

A central finding was that the regulation by cytoplasmic processes of most mitochondrial fluxes, as well as the concentrations of metabolic intermediates, was exerted through ATP_i via the ANT, as illustrated by the response coefficients shown in Table 4. Quantitatively, this result is explained by the large elasticity that the ANT displays toward ATP_i, consistent with its role as the mediator of ADP/ATP exchange between mitochondria and the cytoplasm (3). Because of the inherent definition of the response coefficients (19), the response of respiration to ATP_i depends on two factors: the extent of control exerted on respiration by the ANT; and the elasticity exhibited by the ANT toward ATP_i.

Mechanistically, the central role of ATP_i in the regulatory dynamics of the ECME is realized through the direct relationship between ATP_i production by mitochondria, and ATP consumption by EC coupling processes. This interpretation is supported by results obtained with a preliminary version of the ECME model in which the integration of EC coupling with mitochondrial energetics was effected only through Ca^{2+} and Na^+ without communication between the adenine nucleotide pools. This type of coupling was insufficient to elicit significant cross talk between the two submodels (S. Cortassa, M. Aon, and B. O'Rourke, unpublished data).

ATP_i was the major regulator of mitochondrial respiration under working conditions and its regulatory effect is mediated through the control exerted by the ANT on ATP synthase and respiration. Indirectly, ATP_i also exerts its regulatory action on mitochondrial functions through the effect on $\Delta\Psi_m$. Even if quantitatively small, the control of $\Delta\Psi_m$ is relevant since all processes that contributed to building up $\Delta\Psi_m$ had a negative effect on respiration, whereas those that consume $\Delta\Psi_m$ exerted positive control over respiration (Fig. 5).

The dependence of respiration on adenine nucleotide levels has been well validated in isolated mitochondria (22), but its assessment in intact tissue has been more difficult to obtain. The problem revolves around the methods typically used to measure bulk ATP and ADP (i.e., chemical extraction or phosphorous NMR). The results obtained with these procedures do not truly reflect the local environment of the enzymes of the mitochondrial inner membrane, such as the ANT or creatine kinase (CK). In intact cells and tissues, the reaction catalyzed by CK both buffers ATP_i and transmits changes in the ATP/ADP ratio from the contractile machinery to the mitochondrion. Hence, the increase in ATP turnover at the myofilament is necessarily accompanied by a similar increase in ADP transport across the inner mitochondrial membrane. Dynamic ADP compartmentation models have been developed to address this issue (23) In this model, the shuttling of the ADP signal from the AM-ATPase sites to the mitochondrial membrane is simulated by incorporation of a separate pool of nucleotides, which responds rapidly to EC coupling-mediated changes. Thus, control by energy demand (the ''pull'' condition described in (11)) is a prominent feature of the ECME model.

Ca^{2+} activation of the TCA cycle dehydrogenases makes a smaller contribution to the control of global cardiac cell function in the model, but it should be emphasized that this mechanism is important for maintaining the steady-state redox potential during periods of increased work (3). This could have potential implications for adaptive or signaling responses sensitive to the cellular redox status (24,25).

Control and regulation by diffuse loops in complex networks

When the pattern of control shown in, e.g., Fig. 2 *A*, is analyzed, it reveals that while control exerted by some processes can be readily interpreted, control by other processes may not be evident on first consideration. The detailed analysis of the two following examples illustrates the type of control that arises when a network is examined as a whole. The control of the flux through a process A (e.g., respiration) by a process B (e.g., V_{Cauni}) is exerted indirectly through an effector (e.g., Ca^{2+}) resulting in an increase of the flux through process C (e.g., TCA cycle) that in turn controls positively the flux through process A. Thus, when the control of A by B is mediated by C, we will name this mechanism as *control by diffuse loops*. Control by diffuse loops may be considered to be a transitive property (if A=B and B=C, then A=C). Thus, due to the inherent interconnectedness between all processes, the potential exists that in a complex network of reactions, control by diffuse loops is very frequent.

Table 3 summarizes some diffuse control loops shown in this work. Let us analyze the positive control on mitochondrial

respiration exerted by the AM-ATPase that, under working conditions, also controls positively the flux through the TCA cycle, and the concentration of NADH (not shown). This control is ultimately mediated by the increase in $Ca^{2+}{}_m$ as a consequence of larger amounts of cytoplasmic Ca^{2+}, $Ca^{2+}{}_i$ (Table 3, first row). The increase in $Ca^{2+}{}_i$, in turn, depends on the decrease in SERCA activity, which is negatively controlled by AM-ATPase (not shown). In a nutshell, both the positive control of AM-ATPase on respiration and NADH is mediated by $Ca^{2+}{}_m$. This control also explains the positive control displayed by AM-ATPase on $Ca^{2+}{}_i$ (not shown).

Another interesting example is given by the control exerted on respiration by the processes participating in mitochondrial Ca^{2+} transport; under working conditions, V_{Cauni} controls positively and V_{NCE} negatively (Fig. 3). Despite the fact that both processes are $\Delta\Psi_m$ consumers, the effect appears to be operating more significantly through mitochondrial Ca^{2+}, $Ca^{2+}{}_m$ (Table 3, second row). The following facts should be considered in order to understand this control: 1), the TCA cycle controls positively respiration; 2), V_{Cauni} and V_{NCE} control $Ca^{2+}{}_m$ positively and negatively, respectively, both under resting and working conditions; and 3), the TCA cycle dehydrogenases display a positive elasticity coefficient with respect to Ca^{2+}. Thus, V_{Cauni} exerts a positive control on respiration because when its activity increases, the subsequent increase in $Ca^{2+}{}_m$ results in a higher flux through the TCA cycle, which then leads to an increase of the electron transport flux through the respiratory chain.

Control and regulation by diffuse loops as applied to the matching between energy supply and demand in the heart

When the network of reactions underlying cardiomyocyte function is assessed as a whole, the concept of control by diffuse loops suggests that the system has evolved with multiple control and regulatory loops. A certain degree of redundancy is expected from such a system, which has to respond robustly over a broad range of physiological stimuli or pathophysiological conditions. Within this framework, a case worth further analyzing is the current controversy concerning the role of Ca^{2+} or adenine nucleotides upon matching between energy supply and demand. One side of the problem concerns the lack of quantitative agreement between the extents of Ca^{2+} activation of respiratory flux observed in vitro as compared with in vivo data. Changes in Ca^{2+} concentration can at maximum, double the respiration (11,26), whereas increases in energy flux of more than an order-of-magnitude higher can be observed in muscle cells in vivo (27). Another facet of the problem relates to the question of matching ATP production and consumption during length-dependent activation of cardiac work without substantial changes in the cytosolic Ca^{2+} transient (27).

Concerning the problems posed, our calculations show that mitochondrial respiration exhibits the highest response toward ATP_i (Table 4). Although the response toward Ca^{2+} was much lower, as compared to ATP_i, diffuse loops dependent on Ca^{2+} affect the levels of ATP_i; in this way, Ca^{2+} affects, indirectly, the respiration through ATP_i. Within this rationale, any process that influences the levels of ATP_i at constant Ca^{2+} will also end up controlling mitochondrial respiration, as exemplified by the Frank-Starling mechanism, where a change in ventricle volume increases respiration at constant amplitude and frequency of Ca^{2+} transients. Additionally, the calculations showed that ADP_i was the second intermediate to which respiration exhibits the highest response coefficient. ATP_i level does not exhibit quantitatively important changes with cardiac workload, but this is not the case for ADP, whose low concentration (μM range) in the cytoplasm is difficult to measure and whose mitochondrial matrix concentration cannot be determined in vivo. Although the concentration of ADP_i has been considered to be fairly constant based on the assumption of equilibrium of the creatine kinase reaction, this may not be the case for ADP_i in the neighborhood of the sites of ATP consumption and ATP production (27).

Taken together, the results presented indicate a direct response of mitochondrial respiration toward ATP_i, and an indirect one with respect to Ca^{2+}, exerted through diffuse loops. Both the high response coefficient of respiration toward ADP_i and quantitatively important local changes in its concentration can account for the matching of energy supply and demand after muscle length-dependent activation of cardiac work. Overall, the control of respiration resides in multiple nodes of the network while a combined action of adenine nucleotides and Ca^{2+} accounts for the regulation of mitochondrial respiration observed in vivo.

Limitations of metabolic control analysis

Metabolic control and its analytical tools have been developed to study the steady state of metabolic systems. Indeed, the derivations in Reder's method are valid only in the neighborhood of a steady state. This issue raises concerns about the application of metabolic control to analyze time-dependent behavior, as in this model. The way we have circumvented this limitation has been to clamp the sarcolemmal membrane potential at +10 mV, a membrane potential that roughly corresponds to the voltage at the plateau phase of the cardiac action potential. The system was allowed to evolve during the clamp to a pseudo-steady state and the control variables were calculated from averages during that period. In contrast, during rest, as there is no pacing, the system evolves toward a steady state. Despite this caveat, this assumption is supported by the work of Ingalls and Sauro (28) in which the validity of applying the tools of metabolic control analysis to averages of time-dependent systems such as those undergoing cyclic variations or rhythms was established. These authors showed that the theorems of metabolic control analysis, such as the summation and connectivity theorems, are fulfilled during time-varying behavior.

Comparison with previous control analyses in whole cells or in tissue

Although metabolic control analysis has been extensively applied to isolated mitochondria from different sources (29,30), few studies have been carried out using intact cells. Ventura et al. investigated the metabolic control of oxidative phosphorylation in isolated mitochondria from liver, revealing a large control coefficient for complex I that increases with age (31). This result is in agreement with our experimental results and theoretical predictions (Fig. 3).

In intact heart, Vogt et al. (32) studied the control and regulation of glycolysis during ischemic preconditioning to understand the mechanisms involved in the protection. Based on the co-response coefficients experimentally determined, new regulatory steps and/or new regulatory mechanisms of glycolytic enzymes had to be invoked to understand the biochemical interactions described. With the assistance of a computational model, and the application of the matrix method for its analysis, the experimental co-responses might be attributed to control by diffuse loops, as described in this work.

In vivo studies performed in skeletal muscle analyzed ^{31}P-NMR data describing changes in high-energy phosphates, ATP and ADP, in the working forearm (33). These authors showed that the actomyosin ATPase exerts a strong control over the ATP turnover at stimulus frequencies up to 1.6 Hz. At higher frequencies, control by mitochondrial ATP production became more prominent. Although this work does not analyze the control at different frequencies, the myofibrillar ATPase is shown to exhibit a high degree of control on mitochondrial respiration that, in turn, is limited by the control exerted by the respiratory chain activity under working conditions.

CONCLUDING REMARKS

Control and regulation in complex reaction networks

The matrix method presented here illustrates the application of tools of metabolic control analysis to networks of processes involving not only metabolic reactions, but electrical and mechanical processes as well. This method may also provide an invaluable tool to assess the functional impact of the overwhelming datasets produced by high-throughput technologies. In addition, this work highlights the need for a combined experimental and modeling approach to deeply understand the control and regulation of mitochondrial energetics in cardiac muscle.

APPENDIX 1: METABOLIC CONTROL ANALYSIS—SOME DEFINITIONS

Given a network of processes of any complexity, the rates of the individual processes constituting such network influence are influenced by the rates of the other constituent processes with which they interact. Metabolic control analysis provides a theoretical and conceptual framework to address questions as to what extent a flux in a network depends on the activity of all other different processes (20,21). To quantify such control, a series of coefficients have been introduced. The most frequently reported value is the flux control coefficient, $C^{J_i}_{E_k}$,

$$C^{J_i}_{E_k} = \frac{\frac{\partial J_i}{J_i}}{\frac{\partial E_k}{E_k}}, \tag{5}$$

with J_i representing the flux of interest, and E_k the activity of process k whose control is quantified by $C^{J_i}_{E_k}$.The flux control coefficient measures how much of the flux through a pathway (e.g., oxygen consumption flux, J_i) or a single step (e.g., adenine nucleotide translocase, J_i) would be modified if any activity in the system changes through either modification in enzyme abundance or activity (e.g., changes in the rate of ATP synthase, E_k). An analogous definition applies for the metabolite concentration control coefficient, $C^{M_i}_{E_k}$.These two coefficients reflect global properties of the network; both are dependent on the rates of all processes in the system. If the magnitude of the control coefficient is close to 1.0, it indicates that a change in the flux (e.g., O_2 consumption rate) will be almost proportional to the change in the activity of the process whose rate has been altered (e.g., electron transport through complex I activity, as in Fig. 3 *B*).

On the other hand, the elasticity coefficient, $\varepsilon^{v_k}_{S_j}$,quantifies the dependence of the rate of a specific process, k, on the concentration of any intermediate or effector in the network, S_J. The elasticity coefficient, as defined in Eq. 6, computes the magnitude by which an enzyme activity (e.g., ATP synthase, v_k) changes upon variation in the level of a substrate or an effector (e.g., ADP, S_j). In contrast to control coefficients, elasticities depend upon local properties of the enzyme, and the concentrations of its substrates and effectors. In practical terms, elasticities correspond to the slope of the plot of the initial rate of an enzyme-catalyzed reaction as a function of its substrate (or an effector),

$$\varepsilon^{v_k}_{Sj} = \frac{\frac{\partial v_k}{v_k}}{\frac{\partial S_J}{S_J}}. \tag{6}$$

(For a more in-depth discussion and development of the analytical tools of MCA, the reader is referred to (19).)

To quantify regulatory interactions with respect to internal or external variables operating in a metabolic network, Ainscow and Brand (16) utilized the response coefficients of, e.g., flux J_i with respect to intermediary x, as

$$R^{J_i}_x = \sum_{\text{all } k} \mathrm{C}^{J_i}_k \, \varepsilon^k_x \,, \tag{7}$$

where $C^{J_i}_k$ is the flux control coefficient with respect to the activity of process k, and ε^k_x the elasticity of the rate of k with respect to the intermediate x. The quantity $R^{J_i}_x$ accounts for the participation of different factors (e.g., metabolites, x) in the mechanisms of control of a variable, such as a flux J_i. Each of the terms in the summation in Eq. 7 highlights the importance of the individual process, k, in the control of variable J_i, and are called partial response coefficient, as follows:

$$^k\mathrm{R}^{J_i}_k = \mathrm{C}^{J_i}_k \, \varepsilon^k_x. \tag{8}$$

APPENDIX 2: MATRIX METHOD OF METABOLIC CONTROL ANALYSIS AS APPLIED TO THE MITOCHONDRIAL ENERGETICS (ME) MODEL

In the matrix method developed by Reder (5), the control and regulation of a biochemical network of processes is calculated from the stoichiometry matrix (N) and the matrix of elasticity coefficients ($D_x v$). In the common case of conservation relationships, the stoichiometric matrix N contains

TABLE 5 Flux control coefficients of each of the fluxes (rows) by individual processes (columns) of the ME model

	V_{TCA}	V_{O2}	V_{HNe}	V_{HFe}	V_{ATPsy}	V_{Hu}	V_{leak}	V_{ANT}	V_{CaUni}	V_{NCE}	Sum
V_{TCA}	0.032	0.921	−0.581	−0.021	−0.034	0.226	0.007	0.109	0.277	−0.005	0.93
V_{O2}	0.032	0.921	−0.582	−0.021	−0.034	0.226	0.007	0.109	0.277	−0.005	0.93
V_{HNe}	0.029	−0.077	0.390	−0.022	−0.035	0.237	0.007	0.114	0.289	−0.004	0.93
V_{HFe}	−0.056	0.008	−0.619	0.978	−0.035	0.241	0.007	0.113	0.280	0.009	0.93
V_{ATPsy}	0.173	−1.226	3.146	0.112	0.229	−1.225	−0.036	1.666	−1.443	−0.027	1.37
V_{Hu}	0.051	−0.197	0.756	0.027	−0.107	0.706	−0.009	0.216	−0.345	−0.008	1.09
V_{leak}	0.002	0.000	0.017	0.001	0.001	−0.007	1.000	−0.003	−0.008	0.000	1.00
V_{ANT}	0.092	0.014	0.993	0.035	0.077	−0.387	−0.011	0.767	−0.450	−0.014	1.12
V_{CaUni}	0.005	−0.001	0.050	0.002	0.003	−0.020	−0.001	−0.009	0.977	−0.001	1.01
V_{NCE}	0.005	−0.001	0.050	0.002	0.003	−0.020	−0.001	−0.009	0.977	−0.001	1.01

rows that are linear combinations of other ones in the same matrix (singular matrix). This property does not allow performing the matrix inversion operations that are required to compute the control coefficient matrices. Thus, a reduced stoichiometric matrix, N_r, has to be introduced, containing only those rows with variables not related through conservation relationships. The complete stoichiometric matrix, N, and the reduced matrix, N_r, are related through a link matrix, L. In the method, the flux control coefficients and the metabolite concentration control coefficients are calculated according to the following linear algebra operations (see also Computational and Experimental Methods):

$$C = Id_r - D_x v\, L \left(N_r\, D_x v\, L\right)^{-1} N_r, \tag{9}$$

$$\Gamma = -L \left(N_r\, D_x v\, L\right)^{-1} N_r. \tag{10}$$

Below we show the structure of the matrices, N_r and $D_x v$, applied to the ME model in which the TCA cycle has been lumped:

$$D_x v = \begin{pmatrix}
\frac{\partial V_{TCA}}{\partial [NADH]} & \frac{\partial V_{TCA}}{\partial \Delta\Psi_m} & \frac{\partial V_{TCA}}{\partial [ADP_m]} & \frac{\partial V_{TCA}}{\partial [Ca^{2+}]} & \frac{\partial V_{TCA}}{\partial [NAD^+]} & \frac{\partial V_{TCA}}{\partial [ATP_m]} \\
\frac{\partial V_{O_2}}{\partial [NADH]} & \frac{\partial V_{O_2}}{\partial \Delta\Psi_m} & \frac{\partial V_{O_2}}{\partial [ADP_m]} & \frac{\partial V_{O_2}}{\partial [Ca^{2+}]} & \frac{\partial V_{O_2}}{\partial [NAD^+]} & \frac{\partial V_{O_2}}{\partial [ATP_m]} \\
\frac{\partial V_{HNe}}{\partial [NADH]} & \frac{\partial V_{HNe}}{\partial \Delta\Psi_m} & \frac{\partial V_{NHe}}{\partial [ADP_m]} & \frac{\partial V_{HNe}}{\partial [Ca^{2+}]} & \frac{\partial V_{HNe}}{\partial [NAD^+]} & \frac{\partial V_{NHe}}{\partial [ATP_m]} \\
\frac{\partial V_{HFe}}{\partial [NADH]} & \frac{\partial V_{HFe}}{\partial \Delta\Psi_m} & \frac{\partial V_{HFe}}{\partial [ADP_m]} & \frac{\partial V_{HFe}}{\partial [Ca^{2+}]} & \frac{\partial V_{HFe}}{\partial [NAD^+]} & \frac{\partial V_{HFe}}{\partial [ATP_m]} \\
\frac{\partial V_{ATPsy}}{\partial [NADH]} & \frac{\partial V_{ATPsy}}{\partial \Delta\Psi_m} & \frac{\partial V_{ATPsy}}{\partial [ADP_m]} & \frac{\partial V_{ATPsy}}{\partial [Ca^{2+}]} & \frac{\partial V_{ATPsy}}{\partial [NAD^+]} & \frac{\partial V_{ATPsy}}{\partial [ATP_m]} \\
\frac{\partial V_{Hu}}{\partial [NADH]} & \frac{\partial V_{Hu}}{\partial \Delta\Psi_m} & \frac{\partial V_{Hu}}{\partial [ADP_m]} & \frac{\partial V_{Hu}}{\partial [Ca^{2+}]} & \frac{\partial V_{Hu}}{\partial [NAD^+]} & \frac{\partial V_{Hu}}{\partial [ATP_m]} \\
\frac{\partial V_{leak}}{\partial [NADH]} & \frac{\partial V_{leak}}{\partial \Delta\Psi_m} & \frac{\partial V_{leak}}{\partial [ADP_m]} & \frac{\partial V_{leak}}{\partial [Ca^{2+}]} & \frac{\partial V_{leak}}{\partial [NAD^+]} & \frac{\partial V_{leak}}{\partial [ATP_m]} \\
\frac{\partial V_{ANT}}{\partial [NADH]} & \frac{\partial V_{ANT}}{\partial \Delta\Psi_m} & \frac{\partial V_{ANT}}{\partial [ADP_m]} & \frac{\partial V_{ANT}}{\partial [Ca^{2+}]} & \frac{\partial V_{ANT}}{\partial [NAD^+]} & \frac{\partial V_{ANT}}{\partial [ATP_m]} \\
\frac{\partial V_{CaUni}}{\partial [NADH]} & \frac{\partial V_{CaUni}}{\partial \Delta\Psi_m} & \frac{\partial V_{CaUni}}{\partial [ADP_m]} & \frac{\partial V_{CaUni}}{\partial [Ca^{2+}]} & \frac{\partial V_{CaUni}}{\partial [NAD^+]} & \frac{\partial V_{CaUni}}{\partial [ATP_m]} \\
\frac{\partial V_{NCE}}{\partial [NADH]} & \frac{\partial V_{NCE}}{\partial \Delta\Psi_m} & \frac{\partial V_{NCE}}{\partial [ADP_m]} & \frac{\partial V_{NCE}}{\partial [Ca^{2+}]} & \frac{\partial V_{NCE}}{\partial [NAD^+]} & \frac{\partial V_{NCE}}{\partial [ATP_m]}
\end{pmatrix}, \tag{11}$$

$$N_r = \begin{pmatrix}
3 & -1 & 0 & 0 & 0 & 0 & 0 & 0 & 0 & 0 \\
0 & 0 & 1 & 1 & 0 & -1 & -1 & -1 & -2 & -1 \\
-1 & 0 & 0 & 0 & -1 & 0 & 0 & 1 & 0 & 0 \\
0 & 0 & 0 & 0 & 0 & 0 & 0 & 0 & 0.0003 & -0.0003 \\
-3 & 1 & 0 & 0 & 0 & 0 & 0 & 0 & 0 & 0 \\
1 & 0 & 0 & 0 & 1 & 0 & 0 & -1 & 0 & 0
\end{pmatrix}. \tag{12}$$

Algebraic operations on these two matrices (indicated in Eqs. 9 and 10) allow the computation of the flux and intermediate concentration control coefficients as well as the response coefficients.

Since the ME model is not merely a biochemical system but also involves transport processes, the applicability of the method has respect to the theorems of metabolic control analysis, although the matrix method does not assume fulfillment of those theorems (5). When applied to a steady state, the summation theorems for the flux and intermediate concentration control coefficients should apply. Tables 5–7 demonstrate agreement with the summation theorems for the ME model.

The deviations of the sum from 1.0 (Table 5 or zero (Table 6) are likely due to the accuracy in the calculation of certain variables. In fact, the summations that display the largest deviation from 1 are those corresponding to ATP synthase and ANT. This is due to the large relative error because of the small value of the concentration of ADP_m compared to the level of ATP_m. (i.e., μM against mM, respectively). Another source of error is given by the lumping of the TCA cycle. ATPsynthase, ANT, and succinate lyase (embedded, in this analysis, in the TCA cycle) are the three processes participating in the equation that rules ADP_m concentration. The lumping of the TCA cycle, introduced for simplicity in the calculations, leads to an error in the quantification of elasticities with respect to ADP_m. This error translates into the computation of the control coefficients for ATP synthase and ANT, thus explaining the deviations of the order of 10^{-1} from the summation theorem.

In Table 7, the values in bold in the diagonal indicate that the summation of the response coefficients (−1.0) for metabolites is fulfilled (16). The fact that metabolites corresponding to the pyrimidine and adenine nucleotide pools (NADH, NAD, ADP, ATP) exhibit half of the value is due to them being subjected to conservation relationships.

TABLE 6 Metabolite concentration control coefficients of each state variable (rows) by individual processes (columns) of the ME model

	V_{TCA}	V_{O2}	V_{HNe}	V_{HFe}	V_{ATPsy}	V_{Hu}	V_{leak}	V_{ANT}	V_{CaUni}	V_{NCE}	Sum
NADH	0.236	−0.238	0.025	0.001	−0.002	−0.010	0.000	0.004	0.025	−0.037	0.003
$\Delta\Psi_m$	0.002	0.000	0.021	0.001	0.001	−0.008	0.000	−0.004	−0.010	0.000	0.003
ADP_m	−0.015	−0.004	−0.157	−0.006	−0.014	0.061	0.002	0.041	0.071	0.002	−0.018
$Ca^{2+}{}_m$	−0.001	0.000	−0.006	0.000	0.000	0.002	0.000	0.001	0.609	−0.606	−0.001
NAD^+	−1.594	1.614	−0.169	−0.006	0.015	0.066	0.002	−0.027	−0.169	0.248	−0.021
ATP_m	0.000	0.000	0.001	0.000	0.000	0.000	0.000	0.000	0.000	0.000	0.000

TABLE 7 Response coefficients of the state variables (rows) with respect to intermediates in the ME model (columns)

	NADH	$\Delta\Psi_m$	ADP_m	$Ca^{2+}{}_m$	NAD^+	ATP_m
NADH	**−0.5**	0.0	0.0	0.0	0.1	0.0
$\Delta\Psi_m$	0.0	**−1.0**	0.0	0.0	0.0	0.0
ADP_m	0.0	0.0	**−0.5**	0.0	0.0	9.4
$Ca^{2+}{}_m$	0.0	0.0	0.0	**−1.0**	0.0	0.0
NAD^+	3.4	0.0	0.0	0.0	**−0.5**	0.0
ATP_m	0.0	0.0	0.0	0.0	0.0	**−0.5**

This work was supported by National Institutes of Health grant Nos. P01HL081427, R33HL87345, and N01-HV-28180.

REFERENCES

1. Saks, V., R. Favier, R. Guzun, U. Schlattner, and T. Wallimann. 2006. Molecular system bioenergetics: regulation of substrate supply in response to heart energy demands. *J. Physiol.* 577:769–777.
2. Balaban, R. S. 2002. Cardiac energy metabolism homeostasis: role of cytosolic calcium. *J. Mol. Cell. Cardiol.* 34:1259–1271.
3. Cortassa, S. C., M. A. Aon, B. O'Rourke, R. Jacques, H. J. Tseng, et al. 2006. A computational model integrating electrophysiology, contraction and mitochondrial bioenergetics in the ventricular myocyte. *Biophys. J.* 91:1564–1589.
4. Brandes, R., and D. M. Bers. 2002. Simultaneous measurements of mitochondrial NADH and Ca^{2+} during increased work in intact rat heart trabeculae. *Biophys. J.* 83:587–604.
5. Reder, C. 1988. Metabolic control theory: a structural approach. *J. Theor. Biol.* 135:175–201.
6. Kacser, H., and J. A. Burns. 1995. The control of flux. *Biochem. Soc. Trans.* 23:341–366.
7. Sauro, H. M., J. R. Small, and D. A. Fell. 1987. Metabolic control and its analysis. Extensions to the theory and matrix method. *Eur. J. Biochem.* 165:215–221.
8. Westerhoff, H. V., and D. B. Kell. 1987. Matrix method for determining steps most rate-limiting to metabolic fluxes in biotechnological processes. *Biotechnol. Bioeng.* 30:101–107.
9. Jafri, M. S., J. J. Rice, and R. L. Winslow. 1998. Cardiac Ca^{2+} dynamics: the roles of ryanodine receptor adaptation and sarcoplasmic reticulum load. *Biophys. J.* 74:1149–1168.
10. Rice, J. J., M. S. Jafri, and R. L. Winslow. 2000. Modeling short-term interval-force relations in cardiac muscle. *Am. J. Physiol. Heart Circ. Physiol.* 278:H913–H931.
11. Cortassa, S., M. A. Aon, E. Marban, R. L. Winslow, and B. O'Rourke. 2003. An integrated model of cardiac mitochondrial energy metabolism and calcium dynamics. *Biophys. J.* 84:2734–2755.
12. Magnus, G., and J. Keizer. 1997. Minimal model of β-cell mitochondrial Ca^{2+} handling. *Am. J. Physiol.* 273:C717–C733.
13. Pietrobon, D., M. Zoratti, G. F. Azzone, and S. R. Caplan. 1986. Intrinsic uncoupling of mitochondrial proton pumps. 2. Modeling studies. *Biochemistry.* 25:767–775.
14. Zoratti, M., M. Favaron, D. Pietrobon, and G. F. Azzone. 1986. Intrinsic uncoupling of mitochondrial proton pumps. 1. Non-Ohmic conductance cannot account for the nonlinear dependence of static head respiration on $\delta\mu$H. *Biochemistry.* 25:760–767.
15. Dos Santos, P., M. K. Aliev, P. Diolez, F. Duclos, P. Besse, et al. 2000. Metabolic control of contractile performance in isolated perfused rat heart. Analysis of experimental data by reaction:diffusion mathematical model. *J. Mol. Cell. Cardiol.* 32:1703–1734.
16. Ainscow, E. K., and M. D. Brand. 1999. Internal regulation of ATP turnover, glycolysis and oxidative phosphorylation in rat hepatocytes. *Eur. J. Biochem.* 266:737–749.
17. Kahn, D., and H. V. Westerhoff. 1991. Control theory of regulatory cascades. *J. Theor. Biol.* 153:255–285.
18. Gellerich, F. N., W. S. Kunz, and R. Bohnensack. 1990. Estimation of flux control coefficients from inhibitor titrations by non-linear regression. *FEBS Lett.* 274:167–170.
19. Fell, D. A. 1996. Understanding the Control of Metabolism. Portland Press, London.
20. Fell, D. A. 1992. Metabolic control analysis: a survey of its theoretical and experimental development. *Biochem. J.* 286:313–330.
21. Cortassa, S., M. A. Aon, A. A. Iglesias, and D. Lloyd. 2002. An Introduction to Metabolic and Cellular Engineering. World Scientific, Singapore.
22. Chance, B., and G. R. Williams. 1956. The respiratory chain and oxidative phosphorylation. *Adv. Enzymol. Relat. Subj. Biochem.* 17:65–134.
23. Vendelin, M., O. Kongas, and V. Saks. 2000. Regulation of mitochondrial respiration in heart cells analyzed by reaction-diffusion model of energy transfer. *Am. J. Physiol. Cell Physiol.* 278:C747–C764.
24. Aon, M. A., S. Cortassa, C. Maack, and B. O'Rourke. 2007. Sequential opening of mitochondrial ion channels as a function of glutathione redox thiol status. *J. Biol. Chem.* 282:21889–21900.
25. Maack, C., and B. O'Rourke. 2007. Excitation-contraction coupling and mitochondrial energetics. *Basic Res. Cardiol.* 102:369–392.
26. Territo, P. R., S. A. French, M. C. Dunleavy, F. J. Evans, and R. S. Balaban. 2001. Calcium activation of heart mitochondrial oxidative phosphorylation: rapid kinetics of mV_{O2}, NADH, and light scattering. *J. Biol. Chem.* 276:2586–2599.
27. Saks, V., P. Dzeja, U. Schlattner, M. Vendelin, A. Terzic, et al. 2006. Cardiac system bioenergetics: metabolic basis of the Frank-Starling law. *J. Physiol.* 571:253–273.
28. Ingalls, B. P., and H. M. Sauro. 2003. Sensitivity analysis of stoichiometric networks: an extension of metabolic control analysis to non-steady state trajectories. *J. Theor. Biol.* 222:23–36.
29. Groen, A. K., R. J. Wanders, H. V. Westerhoff, R. van der Meer, and J. M. Tager. 1982. Quantification of the contribution of various steps to the control of mitochondrial respiration. *J. Biol. Chem.* 257:2754–2757.
30. Rossignol, R., T. Letellier, M. Malgat, C. Rocher, and J. P. Mazat. 2000. Tissue variation in the control of oxidative phosphorylation: implication for mitochondrial diseases. *Biochem. J.* 347:45–53.
31. Ventura, B., M. L. Genova, C. Bovina, G. Formiggini, and G. Lenaz. 2002. Control of oxidative phosphorylation by Complex I in rat liver mitochondria: implications for aging. *Biochim. Biophys. Acta.* 1553:249–260.
32. Vogt, A. M., M. Poolman, C. Ackermann, M. Yildiz, W. Schoels, et al. 2002. Regulation of glycolytic flux in ischemic preconditioning. A study employing metabolic control analysis. *J. Biol. Chem.* 277:24411–24419.
33. Jeneson, J. A., H. V. Westerhoff, and M. J. Kushmerick. 2000. A metabolic control analysis of kinetic controls in ATP free energy metabolism in contracting skeletal muscle. *Am. J. Physiol. Cell Physiol.* 279: C813–C832.